JACS
JOURNAL OF THE AMERICAN CHEMICAL SOCIETY
Article
pubs.acs.org/JACS

Computational Study on the Working Mechanism of a Stilbene Light-Driven Molecular Rotary Motor: Sloped Minimal Energy Path and Unidirectional Nonadiabatic Photoisomerization

Fengyi Liu and Keiji Morokuma*

Fukui Institute for Fundamental Chemistry, Kyoto University, Kyoto 606-8103, Japan

Supporting Information

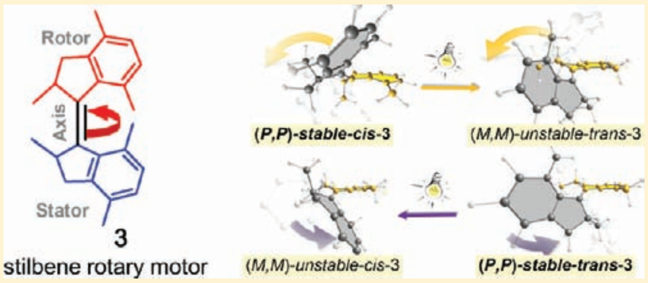

ABSTRACT: The working mechanism of a geometrically overcrowded, chiral stilbene light-driven molecular rotary motor [(2*R*,2*R*)-2,2′,7,7′-tetramethyl-1,1′-bis(indanylidene), **3**] has been investigated by a potential energy surface (PES) study. The reaction paths of the two photoinitiated *cis*−*trans* (or *E*/*Z*) isomerization processes, namely, (*P*,*P*)-*stable-cis*→(*M*,*M*)-*unstable-trans*-**3** and (*P*,*P*)-*stable-trans*→(*M*,*M*)-*unstable-cis*-**3**, have been explored at the CASPT2//CASSCF level of theory. The minimal energy reaction paths (MEPs) of these two processes are nearly parallel on the PESs, separated by a ridge of high inversion barrier. The MEPs have a remarkably steep slope, which drives C═C bond rotation unidirectionally. The asymmetric bias on the excited-state MEPs is caused by the substituents on the "fjord" region as well as by the phenyl moieties. The overall photoisomerization reaction can be described as a three-state (1B→2A→1A) multimode mechanism: The molecule excited to the 1B state first crosses one of the sloped 1B/2A seams, and then follows two cooperative torsional reaction modes to cross preferentially one of the two 2A/1A conical intersections to reach the isomerized ground-state product.

1. INTRODUCTION

Biological molecular motors (molecular machines) are among the most delicate creations in nature. By converting external energy to mechanical force, they work as engines inside cells to power diverse biological cellular functions and sophisticated activities of living creatures.[1] Although construction of artificial molecular devices mimicking the operation of biological molecular motors has yet to be achieved due to their extreme complexity, chemists have been able to design molecular systems with a few relatively simple components and to control the relative motions of the components. Following the syntheses of artificial linear[2] and rotary molecular motors,[3] artificially synthesized molecular motors that are stimulated by different energy inputs and perform different functions have received widespread interest in the past decade.[4] These representative prototypes not only demonstrate state-of-the-art synthetic techniques, but also carry genius ideas that will undoubtedly lead to nanoscale molecular devices in the foreseeable future.

Among various types of artificially designed systems, light-driven rotary molecular motors, originally designed by the Feringa group, have attracted special interest.[5] These molecules undergo repetitive and unidirectional rotation in a manner similar to that of their biological counterparts, e.g., bacterial flagella and ATPase. Light is an ideal source of energy for molecular motor, superior to many other energy inputs (e.g., thermal, chemical, and electrochemical energies). It has many advantages, such as being clean, easy-to-control (intensity, wavelength, distance, etc.), and highly selective. Therefore, light-driven molecular motors are among the most promising classes in applications. In addition, nature has provided many elegant examples of how light manipulates electronic states of molecules and generates reversible and repetitive processes. Through these examples we have learned that the electronic and geometrical structures of excited states can be remarkably different from those in the ground state; it is possible to utilize these differences to stimulate molecular motions in properly designed systems. For example, the light-driven rotary motors designed by Feringa's group were obtained mainly by exploiting the carbon−carbon photoisomerization in helical overcrowded alkenes.[5] Tuning the nondirectional/bidirectional C═C bond rotation to a directional pattern requires an in-depth understanding of the potential energy surfaces (PESs) in different electronic states, especially the excited-state ones. Unfortunately, information about the excited-state ultrafast photochemical processes of the involved molecules, which could be obtained from time-resolved spectroscopy or high-level theoretical calculations, has never been sufficient, not to mention the subtle nonadiabatic processes governed by the interactions between the PESs which play crucial roles in determining the reaction path and branching ratio of the photoproducts:[6] i.e., conical intersections (CIs) in $f - 2$ degrees of freedom (f = degrees of freedom) when the two states have

Received: December 7, 2011
Published: February 13, 2012

the same spin and symmetry, or seams of crossing (SXs) in $f-1$ degrees of freedom when the two states have different spin or symmetry.

Despite the evident challenges associated with light-driven rotary motors, theoretical efforts, including PES calculations and molecular dynamics (MD) simulations, have started to emerge recently. In 2009, Torras et al.[7] reported a DFT and MP2 study on the ground-state rotational profiles of a molecular "gearbox" [9-(2,3-dihydro-2-phenyl-1*H*-benz[*e*]-inden-1-ylidene)-9*H*-fluorene]. Later, Kazaryan et al. reported their calculation on the ground (S_0) and first excited singlet (S_1) states of an overcrowded biphenanthrylidene [(3*R*,3′*R*)-(*P*,*P*)-*trans*-1,1′,2,2′,3,3′,4,4′-octahydro-3,3′-dimethyl-4,4′-biphenanthrylidene] molecular motor by state-averaged spin restricted ensemble-referenced Kohn−Sham (SA-REKS) methods,[8a] and on its excited-state dynamics by a classical OPLS force field method[8b] and semiclassical surface hopping dynamics with a semiempirical quantum mechanics Hamiltonian (OM2/GUGA-MRCI).[8c] These calculations revealed interesting features of the rotary profiles in a light-driven molecular rotary motor. Still, we found it necessary to carry out multiconfigurational ab initio calculations to describe the primary events of the photoisomerization taking place on the excited-state surface, and to reveal the role of the "dark state" in the *cis*−*trans* photoisomerization processes of conjugated molecules.[6d]

In 2008, a light-driven rotary molecular motor (**3**, Chart 1) based on stilbene (**1**, Chart 1) was synthesized by the Feringa group.[9] This molecule, which has simple geometry but shows an amazing unidirectional, 360° rotation around the central C═C bond (Figure 1), was used as a parent compound in their previous syntheses of molecular rotary motors.[5] Further, its application in chiral catalysis was recently demonstrated by the same group.[5i] As shown in Figure 1, the rotational process consists of four steps, two of which occur in the electronically excited state and involve *cis*−*trans* isomerization of the carbon−carbon bond. The other two thermal helix inversion steps (steps 2 and 4 in Figure 1) have been calculated at the RI-MP2/TZVP//B3LYP/6-31G* level by Pérez-Hernández and González.[10] Their calculation confirmed the unidirectionality of the helical inversion and suggested an asynchronous mechanism for the thermal steps; that is, in step 2 from *unstable-trans*-**3** (called "unstable" following the experimental paper[9] but actually a "less stable" minimum) to *stable-trans*-**3** and step 4 from *unstable-cis*-**3** to *stable-cis*-**3**, the thermal isomerization takes place though asymmetric transition states, whereas the minima of the rotary cycle all present C_2 symmetry. In the meantime, the excited-state PESs of the rotary motor, which are important in rationalizing the chemical nature of the currently synthesized rotary molecular motor and designing new promising motors, have yet to be revealed.

Chart 1

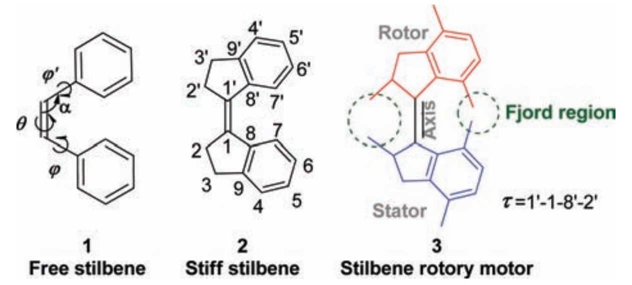

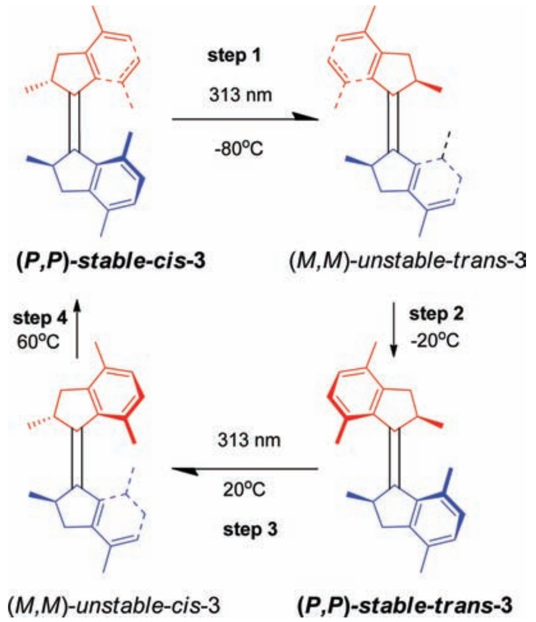

Figure 1. Light-driven four-step rotation scheme in stilbene rotary motor **3** ((2*R*,2*R*)-2,2′,7,7′-tetramethyl-1,1′-bis(indanylidene) (from ref 9). Experimental conditions: step 1, irradiation with 313 nm of a hexane solution of *stable-cis*-**3** at −80 °C; step 2, warming $CDCl_3$ solution at −20 °C for 20 min; step 3, Irradiation of a benzene-d_6 solution of *stable-trans*-**3** at 313 nm and room temperature; step 4, heating the solution from step 3 at 60 °C for 2 h.

In the present study, we explore the photoinduced rotary paths of stiff stilbene molecular motor **3** in the excited states and characterize the interaction between the PESs of the involved electronic states by carrying out complete active space self-consistent field (CASSCF)[11] and complete active space second-order perturbation theory (CASPT2)[12] calculations. Specifically, we studied step 1 of Figure 1, *stable-cis*-**3** to *unstable-trans*-**3**, and step 3, *stable-trans*-**3** to *unstable-cis*-**3**. In order to clarify the role of the constraint and substitution effects, the corresponding photoisomerization steps in its parent compounds, i.e., "free" stilbene **1** and a ring-fused analogue, 1,1′-bis(indanylidene), or the "stiff" stilbene **2**, are also investigated for comparison. The findings of the present study are expected to shed light on the unidirectionality of the photoinitiated C═C rotation processes and the working mechanism of the stilbene molecular motors.

2. COMPUTATIONAL DETAILS

The geometries of the ground state and three low-lying singlet excited states of stilbene rotary motor **3** were optimized at the CASSCF level of theory with the 6-31G basis set.[13] A previous photodynamic experiment suggested that although both the singlet and triplet mechanisms are present in the *cis*−*trans* photoisomerization of stilbene, the singlet mechanism is prevalent in alkyl-substituted stilbenes. (For instance, as one example, the singlet vs triplet yields for unsubstituted stilbene, **1** in Chart 1, are 0.52(*trans*-to-*cis*):0.35(*cis*-to-*trans*):0.002(triplet) for isomerization.)[14] This is understandable since the photoisomerization of stilbene typically takes place within ~1 ps, which is too short to allow for populating the triplet state. Therefore, in the current study, only singlet excited states were considered.

A C_2 symmetry constraint was applied in all CASSCF and CASPT2 calculations (except for optimization of the minima of CIs, which has

Table 1. Key Geometric Parameters (Dihedral Angles θ and φ and Bond Angle α, in Degrees) and CASSCF Relative Energies (kcal/mol)[a] for the Ground- and Excited-State Minima of Free Stilbene 1 and Stiff Stilbene 2

	geometric parameters			relative energies			
structure	θ	φ	α	1A	1B	2A	2B
			Free Stilbene **1**				
***1cis*-1A**	4.2	43.5	129.3	4.2	143.3	144.7	166.9
***1trans*-1A**	180.0	0.0	126.9	0.0	132.4	131.4	150.1
***1perp*-1B**	93.2	−3.8	124.5	52.0	119.8	120.2	148.3
***1trans*-1B**	180.0	0.0	126.1	9.2	120.7	122.5	–
***1cis*-2A**	22.5	9.7	122.4	77.0	142.1	109.2	165.5
***1trans*-2A**	180.0	0.0	126.4	22.8	131.0	108.5	148.0
			Stiff Stilbene **2**				
***2cis*-1A**	7.4	22.4	131.9	2.4	136.6	136.2	149.0
***2trans*-1A**	−179.1	16.0	128.0	0.0	133.3	132.9	153.1
***planar-2trans*-1A**	180.0	0.0	128.2	0.6	132.2	132.6	152.7
***2perp*-1B**	93.3	−3.1	127.1	48.8	117.7	118.0	146.0
***2cis*-2A**	43.0	6.0	128.1	29.4	123.9	105.7	140.3
***2trans*-2A**	149.7	−11.6	128.1	30.4	127.5	110.1	147.3

[a] The energies are relative to the global minima of compounds **1** and **2**, respectively.

been performed without symmetry) in order to minimize the substantial cost of computation. Our preliminary calculations with the density functional B3LYP method suggest that the *cis*- and *trans*-conformers of the molecule and the representative structures along the C_1-C_1' bond rotary profile are mainly symmetric around a C_2 axis (through the bisector of the dihedral angle between two benzene moieties), as shown in Figure S1 (Supporting Information). This was further justified by the recent report by Pérez-Hernández and González.[10]

The state-averaged CASSCF (SA-CASSCF) model was used, allowing for a balanced description of the investigated states, especially at the closely interacting region. The four lowest singlet states included in the C_2 SA-CASSCF wave function are the close-shell ground state (1A), the two lowest spectroscopic B states (1B and 2B), and the "dark" 2A electronic excited state. These four states are adequate for describing the photoisomerization of stilbene, since typically the molecule is excited to either the 2B or 1B state (see section 3).

An active space, with 10 electrons distributed in 10 π orbitals (the π/π^* orbitals of the central ethylene bond, the two degenerate HOMO and LUMO orbitals of each of the two phenyl moieties), denoted as CAS(10,10), was constructed and is illustrated in Figure S2. During the rotary process, the nature of individual orbitals changes significantly, but as a whole, the active orbitals are well conserved against the geometrical variations. In order to locate the minimum-energy paths (MEPs) on the ground- and excited-state PESs along the C1−C1′ rotary profile, a series of constrained geometry optimizations were performed on 1A and 1B states in which the excited- and ground-state isomerizations take place, respectively. Using the minima structures as starting points, we carried out geometry optimizations along the C8−C1−C1′−C8′ dihedral angle (θ in Chart 1) with an initial interval of 30° to identify the one-dimensional rotary potential energy curves (PECs). For some crucial regions, more grids were inserted to ensure the continuity of the curve. However, in photoisomerization of stilbene, the rotary path does not simply correspond to an ethylene-like one-dimensional PEC. Due to the strong interaction between the two phenyl moieties (especially in the *cis*-region), the out-of-plane torsions around C1−C8 and C1′−C8′ also make major contributions in shaping the PES. Therefore, for each θ dihedral angle, local minima considering the C7−C8−C1−C1′ dihedral angle (φ in Chart 1; and φ' = C7′−C8′−C1′−C1, which is same as the former under a C_2 symmetry constraint) were explored. In general, two isomers with different φ dihedral angles can be optimized, one corresponding to the geometry of the *stable-cis→unstable-trans* isomerization step (step 1 in Figure 1) and the other to that of the *stable-trans→unstable-cis* isomerization step (step 3 in Figure 1). Therefore, two valleys on the global two-dimensional PES of **3** (with respect to θ and φ) were located for the 1A and 1B states, respectively. The rotary reaction paths of free stilbene **1** and stiff stilbene **2** were obtained by the same computational strategies.

Along the C=C bond rotation pathways, the investigated states approach each other; therefore, the minimal energy seams of crossing (MSXs)[15] or minimum energy CIs[16] were located at the CASSCF level between the S_2/S_1 (1B/2A) and S_1/S_0 (2A/1A) pairs of PESs. The nature of the CIs was characterized by the branching space calculation that provides the energy gradient difference vector and derivative coupling vector of the molecule at the geometry of the CIs.[16] The energies with dynamic correlation were calculated at the CASPT2 level at CASSCF-optimized geometries (CASPT2//CASSCF), using an internally contracted version (*RS2c*)[17] of the CASPT2 method implemented in MOLPRO 2006.1.[18] In all CASPT2 calculations, a level shift of 0.3 au was applied to avoid the intruder-state problem.[19]

3. RESULTS AND DISCUSSION

The *cis*−*trans* photoisomerization of stilbene is one of the most extensively investigated subjects in photochemistry, both experimentally[20] and theoretically.[21] It has been discovered experimentally[20] that both the *cis*→*trans* and *trans*→*cis* photoisomerizations can take place in stilbene. For instance, for *cis*-stilbene **1**, photodynamic experiments suggested that, at short wavelength (~270 nm), the initial excitation populates the 2B state, followed by an ultrafast relaxation to the 1B fluorescent region, while at longer wavelength (>300 nm), the excitation mainly populates the 1B state, in which the *cis*−*trans* photoisomerization mainly takes place. Both the *cis*- and *trans*-isomers in the 1B state are considered to go down to the ground state near the 1B perpendicular minimum. Therefore, the shapes of the PESs around the Franck−Condon region on the 1B state (1B-FC) and that toward the 1B minimum control the directionality of the photoinitiated C1=C1′ rotation.

The absorption spectra of the *cis*- and *trans*-stilbenes (free stilbene **1**) have been evaluated theoretically by several high-level calculations, including the expensive MS-CASPT2-(14,14)/ANO-L treatments.[21c] The MS-CASPT2 results by Gagliardi and co-workers suggested that vertical excitation from the ground-state *trans*-stilbene is allowed for two B states, both corresponding to $\pi-\pi^*$ excitation. The strongly absorbing state (1B) mainly results from the HOMO→LUMO excitation centered on the C=C bond [labeled as B(HL)], while the weakly absorbing one results from the combination of the local excitation on the phenyl groups [denoted as B(−)]. The 2A state is similar in nature to B(−) but is spectroscopically forbidden. Our CASSCF wave functions at the ground-state minima of stilbene **1**−**3** largely confirmed these findings, although the natures of the B(HL) and B(−) states are found to be mixed.

Compared with the photochemistry of free stilbene **1**, the spectroscopy and photoisomerization processes of ring-fused stiff stilbene **2** and rotary motor **3** have rarely been theoretically documented. Therefore, we calculated the vertical excitation properties of rotary motor **3** at the CASPT2 (gas-phase) and TDDFT (in hexane) levels and summarized the results in Table S1. The simulated absorption spectra as well as the experimental UV spectra (from ref 9) are illustrated in Figure S3. The computed vertical excitations, based on both the CASSCF-optimized structures and the reported crystalline structures, are in good agreement with the reported experimental ones. (For detailed discussion, please refer to the Supporting Information.) From these spectroscopic properties of **3**, it is seen that, at the experimental excitation wavelength (313 nm) reported in ref 9, the molecule is most likely to be excited to the 1B state (rather than the 2B state).

In the following, we will first present the CASSCF-optimized structures on the 1A, 1B, and 2A states for the three stilbenes **1**−**3** (section 3.1). Next, we will briefly present the CASSCF-computed *cis*−*trans* rotary profiles of free stilbene **1** and stiff stilbene **2** in the 1A and 1B states, as well as the directionalities of rotation in *cis*→*trans* and *trans*→*cis* photoisomerization (section 3.2). In sections 3.3 and 3.4, we will focus on the two photoisomerization steps of **3**, i.e., *(P,P)-stable-cis*→*(M,M)-unstable-trans*-**3** (step 1 of Figure 1) and *(P,P)-stable-trans*→*(M,M)-unstable-cis*-**3** (step 3), respectively. Finally, we will propose a working mechanism for a stilbene rotary motor (section 3.5).

3.1. Optimized Structures and Spectroscopic Properties of Stilbenes 1−3.

Table 1 summarizes important geometrical parameters and relative energies for all stationary points optimized on the 1A, 1B, and 2A PESs of free stilbene **1** and stiff stilbene **2**.

*3.1.1. Free Stilbene **1**.* Two ground-state isomers, ***1cis*-1A** (stands for compound **1**, *cis*-conformer, in the 1A state, similarly hereinafter) and ***1trans*-1A**, were located for **1** at the CASSCF/6-31G level of theory. The global minimum ***1trans*-1A** has a totally planar (C_{2v}) geometry, while ***1cis*-1A** is 4.2 kcal/mol less stable and shows a helically twisted C_2-symmetric structure. Due to the steric repulsion between the two phenyl moieties, the central C1−C1′ bond (torsional angle θ) and its neighboring C1−C8 (and C1′-C8′ in the assumed C_2 symmetry) bonds (torsional angle φ) are forced to twist out-of-plane in a synchronous manner. The ***1cis*-1A** ($\theta = 4.2°$, $\varphi = 43.5°$) conformer in Table 1 corresponds to right-hand (*P,P*)-helicity (or more specifically, right-hand axial chirality), and there exists another ***1cis*-1A** ($\theta = -4.2°$, $\varphi = -43.5°$) showing (*M,M*)-helicity. These two helical *cis*-isomers are mirror structures, having identical energies and indistinguishable UV−vis spectra; therefore, in the following discussion, only the (*P,P*)-helical isomer will be mentioned. In the 1B state, the planar *trans*-isomer ***1trans*-1B** has been found, but the corresponding *cis*-isomer does not exist. In addition, a perpendicular ($\theta = 93.2°$) intermediate ***1perp*-1B** has been found with a very small φ dihedral (−3.8°), suggesting full release of the repulsion between the two phenyl moieties. The two minima (***1cis*-2A** and ***1trans*-2A**) on the 2A PES have geometrical features similar to those in the 1A state. The calculated results are quite consistent with previous multi-reference CASSCF calculations.[21]

*3.1.2. Stiff Stilbene **2**.* Introduction of two 5-membered rings into free stilbene **1** produces a stiff stilbene **2**. The 5-membered rings in **2**, hindering the rotation (φ) around the C1−C8 (and C1′−C8′) bonds and constraining the bend of the C1′−C1−C8 (and C1−C1′−C8′) bond angle (α in Chart 1), make the molecule “stiffer”. As a result, they not only prohibit the photocyclization side reaction (which is the predominant side process in free stilbene **1**) but also make a hula-twist (HT) mechanism less feasible. The *cis*−*trans* isomerization of stiff stilbene **2** follows the one-bond-flipping mechanism,[20b] which is the foundation for the directional rotation to be discussed below. Our CASSCF geometry optimization shows this constraint has significant structural and energetic effects on both the ground- and excited-state PESs of **2**.

From Table 1 it is seen that the *P*-helical *cis*-isomer (***2cis*-1A**) has larger θ (7.4°) and smaller φ (22.4°) dihedral angles compared with its counterparts in free stilbene **1**, already reflecting the constraint effects of the 5-membered rings. More significant influences were found on the *trans*-conformers. Two ground-state isomers with similar θ (∼180°) but different φ dihedral angles were located for the *trans*-isomer of **2** (see Table 1). The slightly twisted conformer, ***2trans*-1A**, is the global minimum of the stiff stilbene, while the planar one (***planar-2trans*-1A**), lying ∼0.6 kcal/mol above, was found to be the transition state between the *P*-helical and *M*-helical conformers. These indicate the competition between the 5-membered-ring constraint and the inherited conjugation effects of stilbene; the former tends to destroy the planarity of the molecule, while the latter prefers to form a planar structure. Therefore, in unsubstituted stiff stilbene **2**, the constraint effect of the 5-membered ring starts to take a hand in reshaping the PES, particularly that near the *trans*-conformer. This constraint effect is also reflected by a twisted (***2trans*-2A**) *trans*-conformer in the 2A state that was originally planar in free stilbene **1**. These changes in planarity from ***1trans*-1A** to ***2trans*-1A** (and those on 2A state) imply a role of the 5-membered rings in designing preferable *trans*→*cis* photoisomerization, since in typical *trans*→*cis* photoisomerization processes (for instance, in free stilbene **1**) the excited *trans*-conformer needs to climb out of a potential well generated by the conjugation effect. In properly designed stiff stilbene systems in which the constraint effect (rather than the conjugation effect) predominantly governs the slope of the PES at the *trans*-side, directional *trans*→*cis* photoisomerization could be achieved.

*3.1.3. Stilbene Rotary Motor **3**.* Molecular rotary motor **3** differs from stiff stilbene **2** by the methyl substitutions in the “fjord” regions. (The “fjord region”, which is frequently used in the Feringa-type molecular rotary motor, represents the overcrowded spatial region between the rotor and stator.) Not only do the four methyl groups at the C7, C7′, C2, and C2′ positions further hinder thermal helical inversion between the (*P,P*)- and (*M,M*)-helical isomers, but, more importantly, the asymmetric substituents at the C2 and C2′ atoms create two geometrically chiral centers (C2 and C2′). In this geometrically chiral molecule, there are *R* and *S* enantiomers. In this study we adopted (2*R*,2*R*′)-(*P,P*)-*cis*-**3** as the reference structure, consistent with experimentalists. For the geometrically chiral (2*R*,2*R*′)-**3**, the (*P,P*)- and (*M,M*)-helical isomers are not mirror structures on either the *cis*- or the *trans*-side.

Table 2. Key Geometric Parameters (Dihedral and Bond Angles, in Degrees) and CASSCF and CASPT2//CASSCF Relative Energies (kcal/mol)[a] for the Ground- and Excited-State Minima of Rotary Molecular Motor 3

	geometric parameters			CASSCF				CASPT2			
structure	θ	φ	α	1A	1B	2A	2B	1A	1B	2A	2B
***stable*-3*cis*-1A**	2.8	40.1	131.9	0.0	136.9	136.2	155.2	0.0	106.9	107.2	110.3
***unstable*-3*cis*-1A**	−25.2	−30.2	128.9	8.2	141.0	139.2	151.2	5.3	108.4	110.6	107.9
***stable*-3*trans*-1A**	−200.7	50.5	127.1	2.4	141.2	141.0	163.5	3.8	112.7	112.6	118.1
***unstable*-3*trans*-1A**	162.5	−37.3	127.4	7.6	141.9	140.7	153.0	5.2	109.9	111.0	112.5
3*perp*-1B	85.9	−2.7	128.4	43.3	111.0	111.0	139.2	41.0	106.2	104.9	112.5
3*perp*-1B′	−98.5	9.1	128.3	40.2	109.5	108.3	137.2	38.4	105.4	102.3	110.0
3*cis*-2A′	−65.3	−5.9	129.9	31.4	114.1	103.7	136.8	26.7	106.9	94.1	105.4
3*trans*-2A′	−135.2	33.1	128.2	44.3	117.0	112.1	143.6	41.4	110.3	102.0	115.5
3*cis*-2A	51.2	18.1	128.4	30.9	117.8	105.7	139.8	26.5	109.6	96.9	105.4
3*trans*-2A	128.1	−19.7	128.7	32.7	116.3	106.0	139.4	28.4	109.7	96.9	106.0

[a] The energies are relative to the CASSCF and CASPT2 energies of the global minima of **3**.

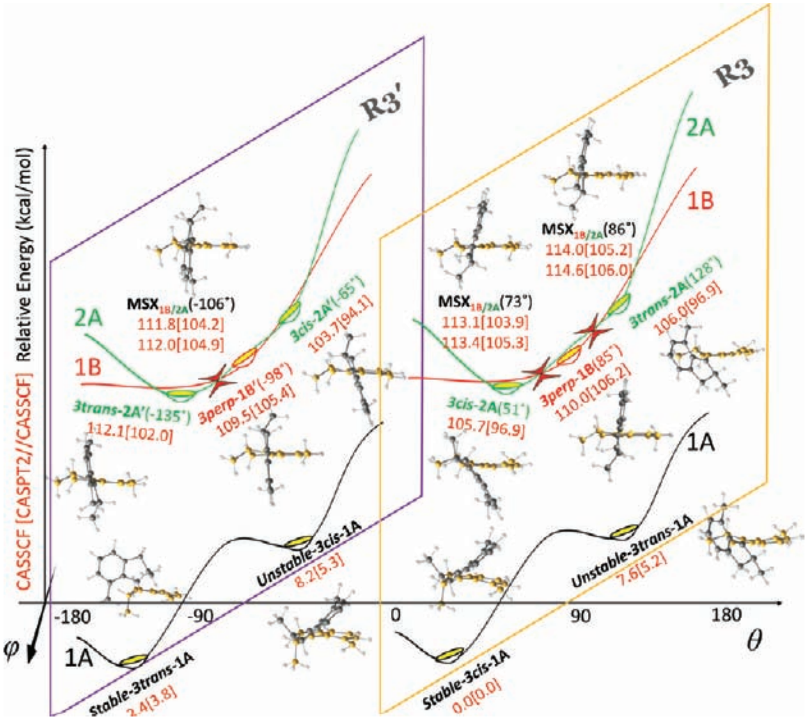

Figure 2. SA-CASSCF-optimized geometries, and the corresponding CASSCF- and CASPT2//SA-CASSCF energies (in square brackets) illustrated in the schematic pseudo-two-dimensional potential profiles of molecular motor **3**. The planes outlined in orange and purple represent qualitative reaction coordinates in the ground state, and as θ increases, φ decreases. **R3** represents rotary isomerization for ***stable-cis→unstable-trans*-3**, and **R3′** represents rotary reaction for ***stable-trans→unstable-cis*-3**. The geometries are shown as top-views according to the stereochemical structures in Figure 1; the C atoms in the "stator" part are shown in brown-yellow, and the C atoms in the "rotor" part are in dark-gray.

The optimized geometries, located in a pseudo-two-dimensional PES with respect to dihedral angles θ and φ (see Chart 1), as well as their relative energies at the CASSCF and CASPT2//CASSCF levels, are summarized in Table 2 and illustrated in Figure 2. As shown in Table 2, four ground-state isomers were located, in good agreement with the experimental characterizations.[9] The two (*P*,*P*)-helical minima (***stable*-3*cis*-1A** and ***stable*-3*trans*-1A**) corresponding to stable conformers in Figure 1 were located at θ = 2.8° and −200.7° (equivalent to 159.3° because of 360° periodicity) along the C1−C1′ rotary profiles, respectively. Meanwhile, the two *unstable* (or *less stable*, called "unstable" following previous papers) (*M*,*M*)-helical minima were also optimized. The energies of these conformers are 8.2 and 7.6 kcal/mol at the CASSCF level and 5.3 and 5.2 kcal/mol at the CASPT2 level, respectively, suggesting balanced relative stabilities, which are prerequisites in designing molecular switches and molecular motors. It is also noticed that the global minimum of the ground state of **3**, in contrast to those (*trans*-conformers) in **1** and **2**, corresponds to a *cis*-conformer (***stable*-3*cis*-1A**); the conjugation effects in the *trans*-side are further decreased in comparison with the 5-membered-ring constraint effect, and as a result no planar *trans*-conformer could be found. On the excited-state PESs, two structurally unique, perpendicular 1B minima and four 2A minima were optimized. The 2A intermediate lies between the 1A and 1B minima along the C1−C1′ rotary path, implying the potential role of the dark 2A state in the photoisomerization processes.

3.2. *Cis*−*Trans* Photoisomerization of Free Stilbene 1 and Stiff Stilbene 2.

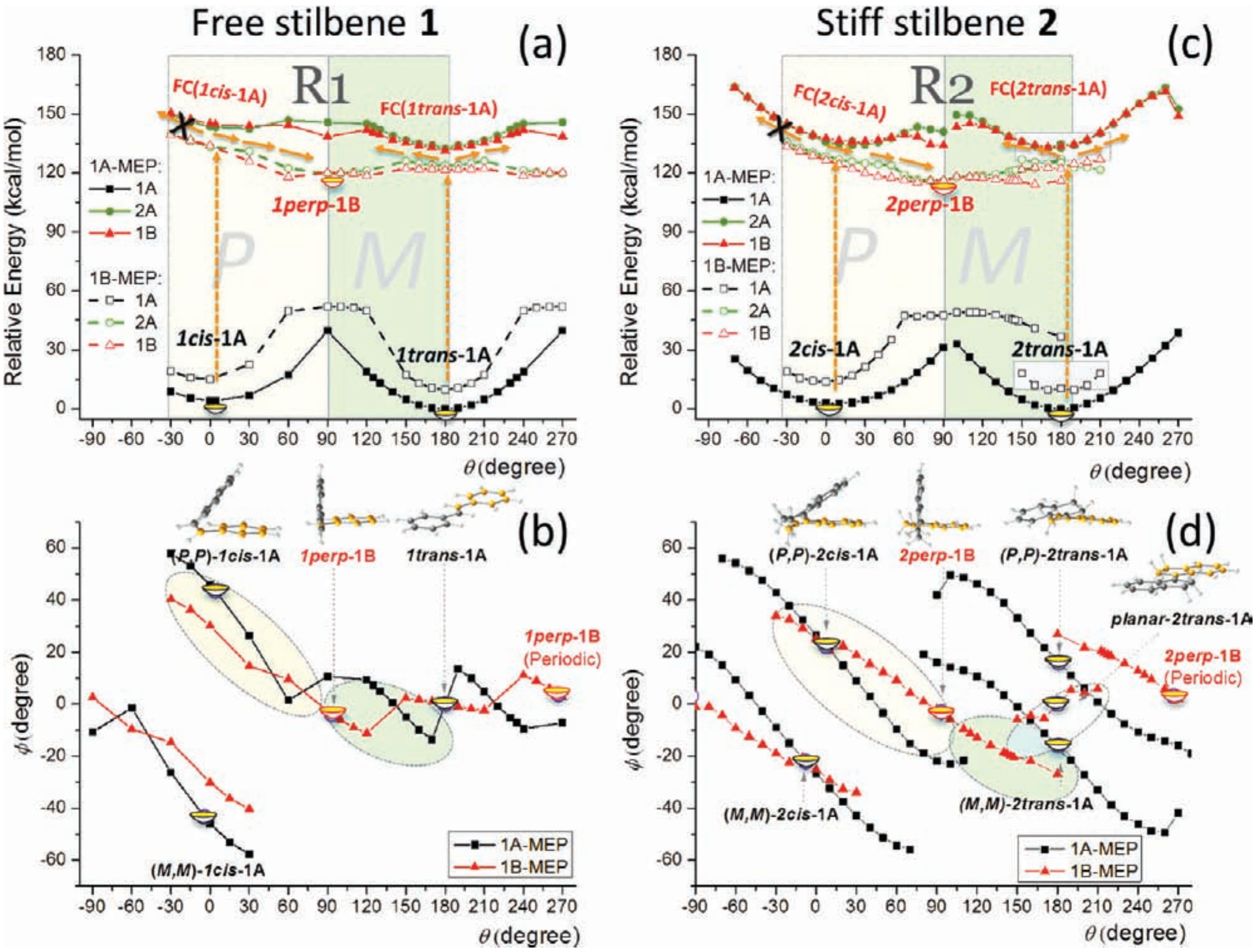

Figure 3. SA-CASSCF-computed minimum energy reaction paths (MEPs) for free stilbene **1** and stiff stilbene **2**. (a) The energies and (b) the variation of the C8−C1 dihedral angle (φ) of 1A and 1B states along the 1A MEP (solid line and filled symbols) and 1B MEP (dashes line and open symbols) as functions of the C1−C1′ torsional angle (θ) for free stilbene **1**; (c) and (d) represent the same for stiff stilbene **2**. The optimized minima on 1A and 1B states are shown as symbols with black and red borders, respectively. The reaction paths emphasized with yellow plane show *P* helicity, while those in green plane follow *M*-helicity. FC denotes the Franck−Condon region. The orange arrows in (a) and (c) indicate the isomerization direction in the 1B state after excitation.

3.2.1. Cis−Trans Photoisomerization of Free Stilbene 1. Figure 3a shows the energy profiles of free stilbene **1** along the rotary MEPs (denoted as reaction **R1**) for the ground 1A (solid symbols) and the excited 1B (hollow symbols) states. The directionality in the forward (*cis*→*trans*) and reverse (*trans*→*cis*) isomerizations is discussed as below.

Cis→Trans Photoisomerization (Directional Rotation). As discussed in section 3.1, for the ***1cis*-1A** isomer, the synchronous torsion of two dihedral angles θ and φ results in two conformers with different helicity. When the molecule is excited to the 1B state, elongation of the C1−C1′ bond and shortening of the neighboring C1−C8 (C1′−C8′) bonds generate a large initial force toward the direction of releasing the strong steric repulsion between the two benzene groups. Therefore, for the individual helical isomer, for example, the **(*P,P*)-*1cis*-1A** employed in this study, the photoinduced C1−C1′ bond rotation is directional. It is seen in Figure 3a that in reaction **R1**, the *cis*→*trans* photoisomerization [following the left-to-right, orange arrows originating at FC(**1*cis*-1A**)] in the 1B state, shown in red curves on either the 1A or 1B MEP, is downhill and essentially barrierless; meanwhile, uphill evolution in the reverse direction [right-to-left orange arrows covered by black “X”, starting from the FC region of ***1cis*-1A**] is not feasible since the rotation is hindered by a high-energetic helical inversion barrier. The descent from the FC region on the 1B PEC drives the excited **(*P,P*)-*1cis*-1A** toward the perpendicular intermediate, accompanied by a continuous increase of the θ dihedral angle. Figure 3b shows the variation of dihedral angle φ against the C1−C1′ rotary angle θ. From **(*P,P*)-*1cis*-1A** to ***1perp*-1B** (black and red curves in yellow region), φ decreases from ~50° to roughly 0°, suggesting an efficient relaxation of the out-of-plane torsion of the benzene moieties. In short, although the *cis*→*trans* photoisomerization can be achieved by both clockwise and anticlockwise rotation, the helical *cis*-**1** indeed prefers, at least in the initial stage, a directional rotary path.

Trans→Cis Photoisomerization (Nondirectional Rotation). As shown in Figure 3a, the *trans*→*cis* isomerization [reaction **R1**, following the right-to-left orange arrows originating from FC(**1*trans*-1A**)] should be slow due to a moderate barrier on the left side of the FC(***1trans*-1A**), trapping the excited ***1trans*-1A** isomer in the 1B state in the well of the FC region; therefore, no evident rotary motion could be generated. It is also seen that the one-dimensional PECs along both the 1A and 1B MEPs in Figure 3a are nearly symmetric with respect to θ = 180°; therefore, the wave packet from the FC region of ***1trans*-**

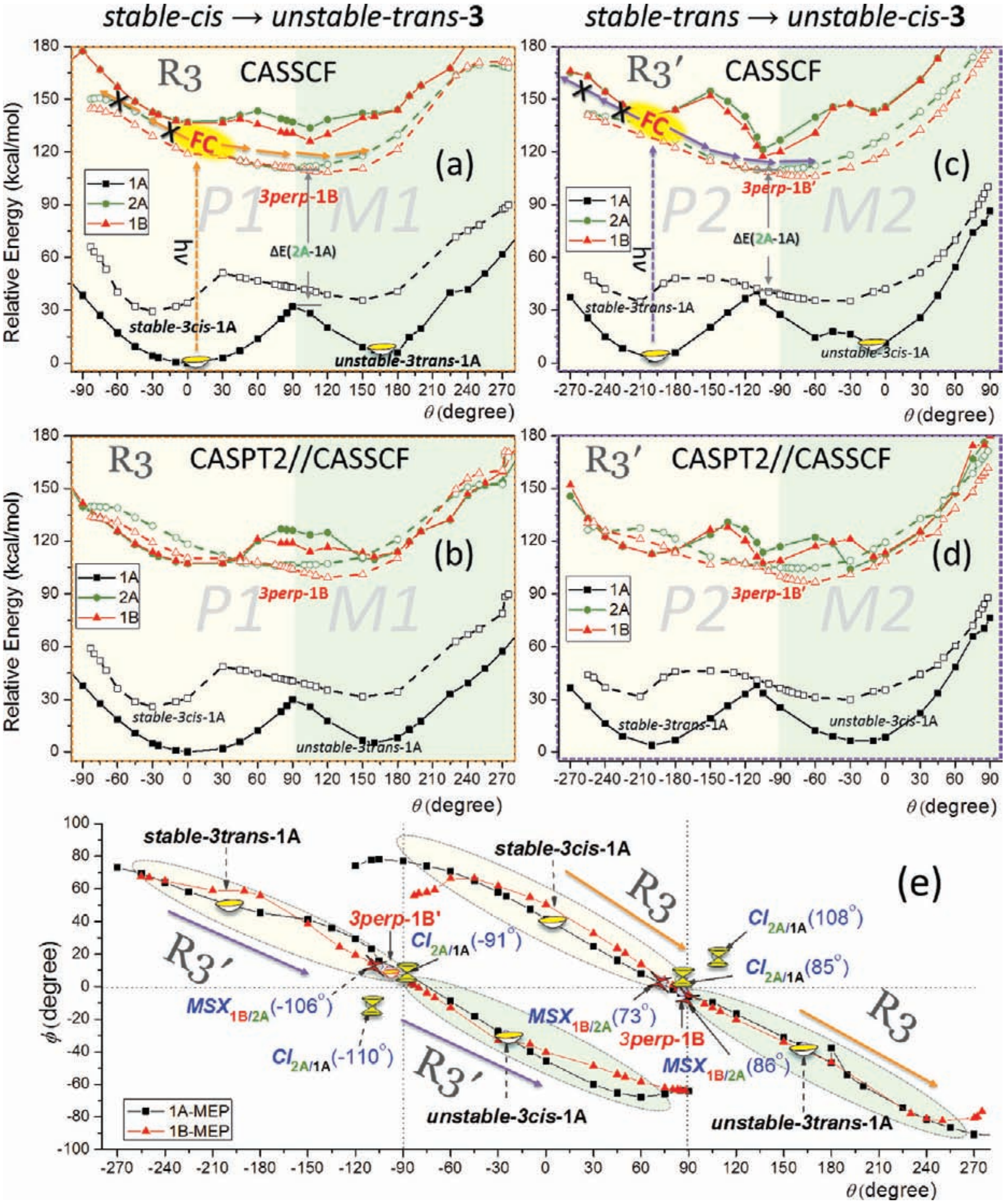

Figure 4. SA-CASSCF (top) and CASPT2//CASSCF (middle) energy profiles of stilbene rotary motor **3**. The 1A MEP (solid line and filled symbols) and 1B MEP (dashed line and open symbols) for the *stable-cis*→*unstable-trans* photoisomerization (step 1 in Figure 1, denoted as the **R3** path) computed at the (a) CASSCF and (b) CASPT2//CASSCF levels (presented in section 3.3). The 1A and 1B MEPs for the *stable-trans*→ *unstable-cis* step (step 3 in Figure 1, denoted as the **R3′** path) calculated at the (c) CASSCF and (d) CASPT2//CASSCF levels (presented in section 3.4). (e) Variation of the C8−C1 dihedral angle φ against the C1−C1′ rotary angle θ along the CASSCF-optimized 1A (black curve) and 1B MEPs (red curve). FC denotes the Franck−Condon region. The orange and purple arrows indicate the direction of isomerization in the 1B state.

1A has equal chances of evolving along the forward or reverse direction to reach two structurally identical perpendicular intermediates. These in total will lead to a slow, nondirectional rotation around the C1−C1′ bond in the *trans*→*cis* isomerization process.

3.2.2. *Cis−Trans Photoisomerization of Stiff Stilbene **2**.*

For stiff stilbene **2**, the CASSCF rotary profiles on the 1A and 1B surfaces (Figure 3c,d) have both similarities and differences with free stilbene **1**.

Cis→Trans Photoisomerization (Directional Rotation). Like in free stilbene **1**, the *cis*→*trans* photoisomerization [see **R2** path in Figure 3c, following left-to-right orange arrows originating from FC(**2*cis*-1A**)] of **2** is a barrierless and directional process. Along the sloped 1B MEP, the dihedral angle φ decreases with the increase of θ, resulting in a helically twisted conformation and the consequent directional momentum. Compared with **R1** in Figure 3a, the steeper slope in the vicinity of FC(**2*cis*-1A**) generates a larger driving force for the *cis*→*trans* rotary isomerization in **2** than in free stilbene **1**.

Trans→Cis Photoisomerization (Nondirectional Rotation). The *trans*→*cis* photoisomerization in stiff stilbene [**R2** path, following right-to-left orange arrows originating from FC-(**2*trans*-1A**)] is more complicated. Competition between the 5-membered-ring constraint and the inherited conjugation effects of stilbene significantly changes the shape of the PESs for both the 1A and 1B states on the *trans* side. Since a helical twisted *trans*-conformer (**2*trans*-1A**), in addition to the planar one (***planar*-2*trans*-1A**), was located on the ground-state PES, the trajectories starting from each FC region possess different characteristics. Trajectories originating from the FC region of the planar conformer (***planar*-2*trans*-1A**), similar to the *trans*→*cis* photoisomerization of free stilbene **1**, are expected to be somehow trapped in a shallow well due to the conjugation effect. The initial reaction path thus presents no directional selectivity (**R2** path in gray box, Figure 3c). Differently, trajectories excited from the helically twisted **2*trans*-1A** minimum show a weak directional initial motion and follow the downhill PES in the direction of the perpendicular 1B intermediate [**R2** path in Figure 3c, following right-to-left orange arrows originating from FC(**2*trans*-1A**)]. Thus, the 5-membered-ring constraints substantially decrease the planarity of the stiff stilbene **2** and partially tune the nondirectional rotation in a directional fashion. Considering the very low thermal helical-inversion barrier (0.6 kcal/mol), however, the *trans*→*cis* photoisomerization in stiff stilbene **2** is considered as rather a nondirectional than a directional rotary process.

3.3. *Stable-Cis→Unstable-Trans* Photoisomerization of Molecular Motor 3.

In the rotary motor **3**, the asymmetric methyl substitutions introduce geometrical chirality into the molecule; thus, only one enantiomer (e.g., *R*-enantiomer in this study) needs to be considered. Starting from the *R*-enantiomer, the two axial helically twisted isomers (which have the same geometric parameters except for the sign of the dihedral angles, as in **1** and **2**), for both the *cis*- and *trans*-sides, become geometrically unique. Therefore, along the helical torsion coordinate, two inequivalent reactions in the full 360° rotary cycle were located on both the 1A and 1B PESs. The two MEPs of *cis*−*trans* isomerization, one corresponding to (*P,P*)-*stable-cis*→(*M,M*)-*unstable-trans*-**3** (step 1 of Figure 1 and reaction **R3** in Figure 4a,b) and the other corresponding to (*P,P*)-*stable-trans*→(*M,M*)-*unstable-cis*-**3** photoisomerization (step 3 of Figure 1 and **R3′** in Figure 4c,d), are calculated at the CASSCF and CASPT2//CASSCF levels and illustrated in Figure 4a−d. The $\varphi-\theta$ geometrical variations along the **R3** and **R3′** are shown in Figure 4e.

From Figure 4e it is clearly seen that the explored **R3** MEPs (discussed in this section) are parallel with **R3′** (to be discussed in section 3.4) on the 2D PESs. Most of the CASSCF-optimized geometries fall into these two valleys (except for two 2A/1A CIs staying within short distance from the MEPs), which justified our geometry optimization strategy in exploring the reaction paths. The two reactive channels, **R3** and **R3′**, are well isolated by a ridge caused by the high helical inversion barrier; thus, the reactive wave packet in one reaction channel has little probability of being repartitioned into the other one. In this sense, the photoisomerizations taking place in these two valleys on the global PES are two separate photoinitiated reactions. Therefore, to make the situation less complicated, we first present the *stable-cis*→*unstable-trans*-**3** (step 1 of Figure 1 and reaction **R3** in Figure 4a,b) photoisomerization in section 3.3, and then present the other photoisomerization step (step 3, *stable-trans*→*unstable-cis*-**3**, corresponding to **R3′** in Figure 4c,d) in section 3.4.

3.3.1. Excited-State Stable-Cis→Unstable-Trans Decay of 3 (1B Dynamics). The *stable-cis*→*unstable-trans* photoisomerization starts from the excited-state 1B-FC structure of *stable-cis*-**3** and ends in ground-state product. Consequently, in the following subsections, we track the evolution of the excited molecule based on qualitative PESs. The excited molecules first slide down along 1B MEP (discussed in this section), then make radiationless transition though 1B→(2A→)1A crossings (discussed in section 3.3.2), and finally reach 1A PES and form the ground-state product. The directionality of the rotation in *stable-cis*→*unstable-trans* photoisomerization is discussed in detail in section 3.3.3.

Both the CASSCF -and CASPT2//CASSCF-computed *stable-cis*→*unstable-trans* 1B MEPs show downhill nature, from the overtwisted ***stable*-3*cis*-1A** FC structures (in 1B state) to isomerized product, ***unstable*-3*trans*-1A** [see **R3** path in Figure 4a, following the left-to-right, orange arrows started from FC(***stable*-3*cis*-1A**)]. Compared to stiff stilbene **2**, the even more sloped 1B MEP in the vicinity of ***stable*-3*cis*-1A** suggests larger initial rotary motion, and thus better directionality of rotation. Also compared with free stilbene **1** and stiff stilbene **2**, it is seen the *stable-cis*→*unstable-trans* photoisomerization of molecular motor **3** shows strong helicity throughout the reaction path. Due to the high inversion barrier between *P*- and *M*-enantiomers caused by the strong repulsions, as discussed in the preceding section, the *P*-helical (***P1*** in Figure 4a, corresponding to *P*-helical regions originating from ***stable*-3*cis*-1A**, shown in yellow background) and the *M*-helical regions (***M1*** in Figure 4a, around the ***unstable*-3*trans*-1A**, shown in green background) are significantly broadened. The overall reaction paths are accompanied by the loss and regain of axial helicity; on the left and right edges of the **R3** PECs, the structures show the largest helical distortions, while in the middle, the perpendicular 1B minima are practically nonhelical.

It is known that for a photochemical reaction starting from an excited state, the reaction pathway, branching ratio of the products, and directionality of motions are governed by the nature and topology of crossings. Although the sloped 1B and partly 1A MEPs in Figure 4a,b suggest a good initial directionality in *stable-cis*→*unstable-trans* photoisomerization, information on PES crossings is needed to determine the overall directionality of the reaction. As shown in Figure 4a,b, both the 1A and 1B MEPs indicate that along **R3** reaction paths, the 2A state (green curves) is close in energy with the 1B state (red curves) in a very broad region, and therefore the 2A state is expected to take part in the nonadiabatic reaction, as suggested by Fuss et al. in the photochemistry of stilbenes.[20b] Therefore, we optimized and characterized the state crossings between the involved states and present the results in the next section.

3.3.2. Nonadiabatic Transition in Stable-Cis→Unstable-Trans Photoisomerization (1B→2A→1A State). 1B/2A Nonadiabatic Transition. Following the reaction profiles **R3**, as shown in orange arrows in Figure 4a, it is found going from the FC region of ***stable*-3*cis*-1A** to the perpendicular intermediate region that the 1B and 2A PECs approach each

Table 3. Key Geometric Parameters (Dihedral and Bond Angles, in Degrees) and CASSCF and CASPT2 Relative Energies (kcal/mol)^a for the Minimum Energy Crossings and Conical Intersections of Rotary Molecular Motor 3

	geometric parameters			CASSCF				CASPT2			
	θ	φ, φ'	α, α'	S_0	S_1	S_2	S_3	S_0	S_1	S_2	S_3
				Stable-Cis → *Unstable-Trans-3*							
$\mathbf{MSX_{1B/2A}}$ (73°)	73.3	3.0, 3.1	127.9, 127.9	45.7	111.1	111.0	–	41.0	106.0	105.2	101.7
$\mathbf{MSX_{1B/2A}}$ (86°)	85.9	−2.6, −2.5	128.4, 128.4	44.0	109.8	109.7	–	39.3	105.3	103.9	100.9
$\mathbf{CI_{2A/1A}}$ (85°)	84.8	4.1, 49.7	135.5, 85.5	136.6	136.7	–	–	118.1	120.7	177.1	184.1
$\mathbf{CI_{\ 2A/1A}}$ (108°)	107.9	19.1, −52.3	126.7, 84.2	134.2	134.2	–	–	114.5	116.3	169.8	178.9
				Stable-Trans → *Unstable-Cis-3*							
$\mathbf{MSX_{1B/2A}}$ (−106°)	−106.0	12.6, 12.5	127.9, 127.9	42.7	108.4	108.4	–	39.0	104.9	104.2	100.7
$\mathbf{CI_{2A/1A}}$(−110°)	−110.2	−10.5, 48.9	126.0, 85.3	130.2	130.2	–	–	110.3	113.6	171.9	177.1
$\mathbf{CI_{\ 2A/1A}}$ (−91°)	−90.9	10.2, −75.3	136.7, 91.7	149.6	149.6	–	–	139.1	139.9	197.1	203.3

^{a}The energies are relative to the absolute CASSCF and CASPT2 energies of the global minima of molecular motor **3**.

other and finally coincide with each other in the vicinities of the 1B minima (***3perp*-1B**). In order to identify the role of the dark 2A state, we optimize the **1B/2A** crossing using the CASSCF methods. Under C_1 symmetry, two state-crossing points [$\mathbf{MSX_{1B/2A}}$**(73°)** and $\mathbf{MSX_{1B/2A}}$**(86°)**; see Table 3 for their key geometric parameters and the CASSCF and CASPT2 relative energies] between the S_1 and S_2 excited-state PESs were located. Technically, these two points located along the gradient difference and derivative coupling spaces should be called S_2/S_1 CIs at C_1 symmetry, since the PESs at these points cross at $f-2$-dimensional hypersurfaces (f is the number of internal degrees of freedom). However, as shown in Figure 4e, both of them (denoted as red "X" icons) practically show C_2 spatial symmetry and lie on the **R3** reaction path (More specifically, $\mathbf{MSX_{1B/2A}}$**(73°)** is located on the left and $\mathbf{MSX_{1B/2A}}$**(86°)** on the right side of the ***3perp*-1B**.) At C_2 symmetry, the S_1 and S_2 states (1B and 2A states) belong to different symmetry and intersect along a $f-1$-dimensional SX. Therefore, the optimized S_2/S_1 crossing points at the C_1 symmetry are actually the minima on a 1B/2A $f-1$-dimensional seam of crossing (MSXs).[15]

Figure 5a,b illustrates the locations of these MSXs [$\mathbf{MSX_{1B/2A}}$**(73°)** and $\mathbf{MSX_{1B/2A}}$**(86°)**, shown as red "X" icon] on the schematic **R3** reaction (light-blue plane). Their gradient difference vectors (GDV, or ***g***) and derivative coupling vectors (DCV, or ***h***) as well as the linear extrapolated PESs along the ***g*** and ***h*** vectors are calculated. A more detailed illustration including these vectors and PESs is provided in Figure S5. ***g*** and ***h*** represent the two directions through which the degeneracy of the two states is lifted and are important in determining the nature of the crossing points. ***g*** and ***h*** of these 1B/2A MSXs are mainly contributed from the vibrations of the phenyl groups [seen from the molecular geometries inside the round-corner boxes and the vectors (red arrows starting from atoms) in Figure S5]. The topology of the MSXs is also clearly identified from the linear extrapolated PESs along the ***g*** and ***h*** vectors. As shown in Figure 5a,b, along the coupled direction of ***g*** and ***h***, the 1B and 2A surfaces (with red and green borders, respectively) coincide in energy along a $f-1$ seam (gray dashed line) and then separate again. The direction of the seams (gray dashed line) is perpendicular to the direction of the 2D reaction path (light-blue plane). These 1B/2A seams and the MSXs provide pathways for the 1B excited state to come down to the 2A excited state. As shown in Figure 5a, following the arrows inside the light-blue reaction plane, the trajectory starting from the FC region of ***stable-3cis*-1A** first travels on the 1B state (red arrows), then crosses the

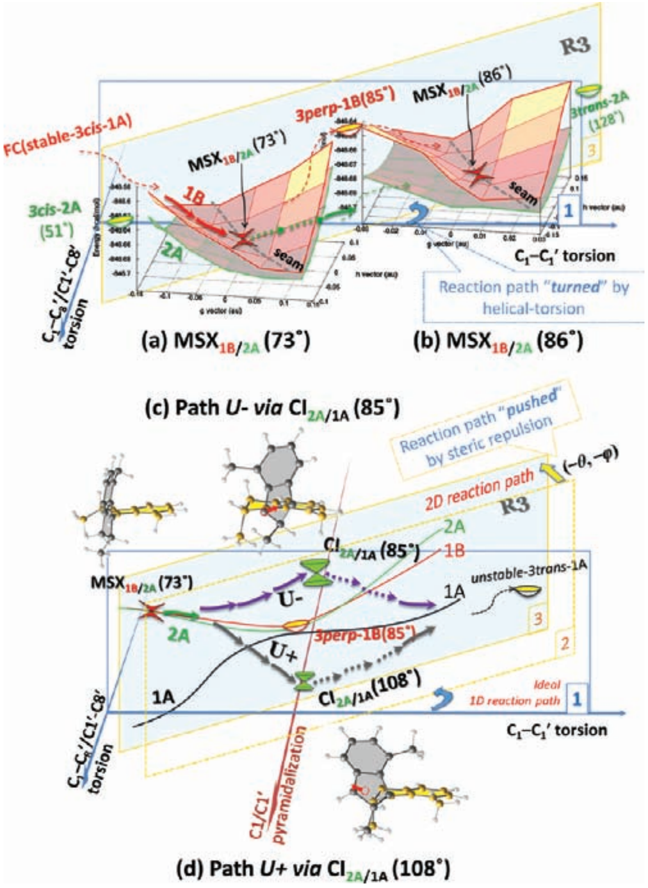

Figure 5. 1B/2A nonadiabatic isomerization reaction paths **R3** on 1B and then 2A PESs via MSXs [(a) $\mathbf{MSX_{1B/2A}}$**(73°)**, (b) $\mathbf{MSX_{1B/2A}}$**(86°)**] and the succeeding pyramidalization reaction paths from 2A to 1A PESs [(c) **U−** via $\mathbf{CI_{2A/1A}}$**(85°)** and (d)**U+** via $\mathbf{CI_{2A/1A}}$**(108°)**] that originated from the **R3** isomerization path (a). The molecular structures of the located crossings are shown with the "stator" in orange and the "rotor" in gray. The PESs in the vicinity of the representative 1B/2A MSXs and 2A/1A CIs are obtained by approximately linear extrapolation along the ***g*** and ***h*** vectors. The blue round arrows mean the "turning" of the reaction coordinate from ideal 1D C−C bond torsion to 2D helical torsional coordinates, and the yellow broad arrows indicate the "direction of pushing" in which the 2D reaction path was "pushed" away from the ideal perpendicular coordinate center by the substitution groups in the "fjord" region in **3**. A detailed illustration including the ***g*** and ***h*** vectors and all linear extrapolated 2D PESs is provided in Figure S5.

$\mathbf{MSX_{1B/2A}}$(73°) (red "X" mark) to reach the 2A PES, and continues (green dashed arrow) along the 2D reaction path. Considering that its relative energy is almost identical with that of the 1B intermediates (111.1 vs 111.0 kcal/mol for 1B minimum at the CASSCF level), the 1B/2A $\mathbf{MSX_{1B/2A}}$(73°) is expected to act as a very efficient funnel through which the molecule on the 1B PES can barrierlessly access the energetically more favorable 2A surface. For the same reason, the second 1B/2A MSX [$\mathbf{MSX_{1B/2A}}$(86°)] in Figure 5b plays a less import role with respect to $\mathbf{MSX_{1B/2A}}$(73°), since the 1B-state trajectories have little probability of reaching this point.

2A/1A Nonadiabatic Transition. After the molecule makes the transition from the 1B state to the 2A state through $\mathbf{MSX_{1B/2A}}$(73°), it reaches a perpendicular region where the 1A and 2A PECs have the narrowest energy gap (indicated by small 2A−1A energy difference in Figure 4a) in the vicinity of ***3perp*-1B** along the **R3** reaction profile. However, this energy gap remains large along the **R3** path, and no efficient nonadiabatic transition to the 1A ground state can take place.

Due to the constraint effect of the 5-membered rings, as discussed in section 3.1, the general HT-type CI in 2A/1A transition of stilbene, which requires large torsion around θ and φ, is unfeasible. Alternatively, it is known in the photochemistry of ethylene and polyenes[6d] that CIs along the C1 and/or C1′ pyramidalization coordinates are also responsible for the 2A/1A crossing. Ideally, the pyramidalization modes are in the direction perpendicular to the C═C bond axis; therefore, the weakening of the double-bond character (of the C═C bond) generally increases the mobility of the C atom along the pyramidalization coordinates. Indeed, starting from the perpendicular ***3perp*-1B** geometry, two S_1/S_0 (2A/1A under C_2 symmetry) minimal energy CIs, namely, $\mathbf{CI_{2A/1A}}$ (85°) and $\mathbf{CI_{2A/1A}}$(108°), were found on either direction of the pyramidalization coordinates. Figure 5c,d illustrates the relative positions of $\mathbf{CI_{2A/1A}}$ (85°) and $\mathbf{CI_{2A/1A}}$(108°) beside the 2D reaction path (light-blue plane). Compared with the C1′−C1−C8′−C2′ pyramidalization angle (τ = 5.7°, see Chart 1 for the definition) in ***3perp*-1B**, the τ angles in $\mathbf{CI_{2A/1A}}$ (85°) and $\mathbf{CI_{2A/1A}}$ (108°) are 27.2 and −28.1°, respectively. These 20−30° variations in τ indicate evident $sp^2 \rightarrow sp^3$ pyramidalization and significant weakening of the conjugation of the molecule (especially the 5-membered ring); therefore, through these 2A/1A CIs, the molecule gains more 1A-like character and has a large probability of reaching the energy-favorable ground state.

The nature of the S_1/S_0 CIs was characterized by the nonadiabatic branching space calculations. One can see from Figure S5c,d that their ***g*** and ***h*** vectors (structures inside round-corner boxes and red arrows originating from atomic centers) are perpendicular with each other and show distinct vibration modes. The ***g*** and ***h*** vectors largely correspond to the out-of-plane distortions of the C1/C1′ and their adjacent atoms (which eventually result in the pyramidalization of the ethylic C1/C1′ atoms), while the C1−C1′ torsion is absent. In addition, the linearly extrapolated PESs scanned along the GDV and DCV suggest that all of these S_1/S_0 CIs have a "sloped" nature (see Figure S5). Moreover, the excited-state molecules need to overcome a 10−30 kcal/mol barrier before they can cross these CIs to reach the 1A surface, which makes the S_1/S_0 nonadiabatic transition less efficient compared with passage through 1B/2A MSXs. In summary, the nonadiabatic *stable-cis→unstable-trans* photoisomerization of **3** could be achieved by the involvement of three states (1B, 2A, and 1A states), two types of crossing (1B/2A MSXs and 2A/1A minimum energy CIs), and two major reaction coordinates (helical torsion and carbon pyramidalization).

3.3.3. Overall Directionality in Stable-Cis→Unstable-Trans Photoisomerization. As discussed above, the formation of a ground-state product could be successfully described by participation of the dark 2A state and the pyramidalized 2A/1A minimum energy CIs. However, the directionality of the C═C bond rotation throughout the 1B→2A→1A radiationless transition process still needs to be rationalized. In general, the involvement of carbon pyramidalization may compromise the directional C═C bond rotation because these two coordinates are perpendicular with each other. As shown in Figure 5c,d, along the positive and negative directions of the pyramidalization axis, the two 2A/1A CIs lie beside the plane of the ideal 1D C═C torsion reaction path. In order to access the ground-state PES, the trajectories are forced to turn to a perpendicular pyramidalization coordinate from the C−C torsion minimal-energy path, and thus trajectories are slowed down and the direction of the rotation may be perturbed.

Despite this drawback, it is found that the *stable-cis→unstable-trans* photoisomerization of overcrowded stilbene rotary motor **3** still shows a good directionality. In the following we provide justification for this retained directionality. First, due to the repulsions between methyl substituents, the *stable-cis→unstable-trans* reaction (**R3**, as shown in Figure 4e, following the orange arrows) cannot be a simple change in the pure "ideal" C1−C1′ torsional angle (θ) but has to accompany a change in the C1−C8 (and C1′−C8′) torsion φ (and φ'), or has to follow a cooperative helical-torsion coordinate composed of both θ and φ (and φ'). Figure 5 illustrates that the real reaction coordinate is not a "pure" C1−C1′ torsion coordinate (on the transparent plane with blue border) but the helical-torsional coordinate (on the transparent plane with yellow dashed border). We will later call this "turning" the reaction coordinate. The helical-torsion reaction plane is not perpendicular to the pyramidalization coordinate. Thus, trajectories following the helical-torsion path have opportunities to reach the pyramidalized 2A/1A CIs without serious loss their inertial velocity and direction of motion.

Second, due to the unbalanced potential caused by the asymmetric substitution, the 2D helical-torsional reaction path has in addition to be "pushed" toward the ($-\theta$,$-\varphi$) direction, indicated by the yellow broad arrow in Figure 5c,d, to result in the reaction coordinate **R3** (on the light blue plane with yellow border). The final 2D reaction coordinate plane is closer to $\mathbf{CI_{2A/1A}}$(85°) but away from $\mathbf{CI_{2A/1A}}$(108°). The close distance between the $\mathbf{CI_{2A/1A}}$(85°) and **R3** reaction path not only increases the probabilities for the 2A trajectories to pass though this CI but also maintains the directionality of the C═C rotation during this process.

Based on the reaction coordinate analyzed above, we showed that the overall 1B→2A→1A radiationless isomerization can take place directionally. As illustrated in Figure 5c,d, 1B-state trajectories first efficiently cross the 1B/2A seam at $\mathbf{MSX_{1B/2A}}$(73°), and the 2A trajectories (green arrows) soon bifurcate following two pyramidalization directions: The reaction path **U−** via $\mathbf{CI_{2A/1A}}$(85°) (purple arrows), rather than the **U+** via $\mathbf{CI_{2A/1A}}$(108°) (dark-gray arrows), is the dominant 2A→1A radiationless transition pathway in the *stable-cis→unstable-trans* photoisomerization of **3**. Since $\mathbf{CI_{2A/1A}}$(85°) is in close vicinity of the 2A reaction paths (light-blue plane), reactive molecules (with some kinetic energy) passing through this CI are expected by and large to maintain the original reaction mode and continue their way toward the product rather than the reactant branch. In short, the 1B→2A→1A nonadiabatic transition in *stable-cis→unstable-trans* photoisomerization of molecular rotary motor **3** is directional.

3.4. *Stable-Trans→Unstable-Cis* Photoisomerization of Molecular Motor 3.

3.4.1. Excited-State Stable-Trans→Unstable-Cis Decay (1B Dynamics). Now that the directionality of *stable-cis→unstable-trans* photoisomerization has been established, the directional *stable-trans→unstable-cis* rotary isomerization, step 3 of Figure 1, is the next key to designing a stilbene rotary motor, since the corresponding processes in its parent compounds **1** and **2** are either nondirectional or poorly directional. Compared with stiff stilbene **2**, in stilbene rotor **3**, the excited-state PES in the vicinity of FC ***stable-3trans*-1A** exhibits no potential well in the 1B MEP (see **P2** region in Figure 4c,d). As indicated by the left-to-right purple arrows in Figure 4c, the sloped FC region generates "good" initial rotary motion. In addition, the *stable-trans→unstable-cis* 1B MEPs are downhill along the whole **R3′** reaction path (left-to-right), suggesting that the *stable-trans→unstable-cis* processes in the 1B state is directional. The same trends were confirmed by the CASPT2//CASSCF energy calculation; from Figure 4d, it is also seen that the dynamic correlation energy does not significantly affect the relative position of the investigated states, although it seems to stabilize the 1A structures more than the 1B ones.

3.4.2. Nonadiabatic Transition in Stable-Trans→Unstable-Cis Photoisomerization (1B→2A→1A State). The nonadiabatic transition from the 1B to 1A state in reaction **R3′** is also studied at the CASPT2//CASSCF level. Table 3 summarizes the geometric parameters and relative energies of 1B/2A MSX and 2A/1A CIs in *stable-trans→unstable-cis* photoisomerization. The mechanism of the nonadiabatic reaction is very similar to the *stable-cis→unstable-trans* transition discussed in section 3.3.2; therefore, it will be discussed very briefly.

Along the **R3′** reaction path (see Figure 4c, purple arrows), the energy gap between 1B and 2A PESs gradually decreases until it reaches the 1B/2A MSX, **MSX$_{1B/2A}$(−106°)**. Figure 6a shows the **R3′** rotary path near the perpendicular intermediate region. (Again, a detailed version of Figure 6 is provided in the Supporting Information as Figure S6.) The **MSX$_{1B/2A}$(−106°)** lies to the left of ***3perp*-1B′** and has energy almost identical with that of ***3perp*-1B′**; after this point, the 1B and 2A PESs are more repulsive. Similar to its counterparts in the **R3** reaction, **MSX$_{1B/2A}$(−106°)** is a very efficient seam through which the molecule on the 1B PESs can barrierlessly access the 2A surface.

Once the molecule accesses the 2A PES, the reaction bifurcates along the C1/C1′ pyramidalization coordinate into two pathways: **V−** [via **CI $_{2A/1A}$(−110°)**, dark-gray arrows] and **V+** [via **CI $_{2A/1A}$(−91°)**, purple arrows], as illustrated in Figure 6b,c. The τ angles (see Figure 1) of these 2A/1A CIs are 31.6 and −21.8°, respectively, and show large variation from the value of 10.9° in ***3perp*-1B′**. Compared to the passages through 1B/2A MSXs, both the **V−** and **V+** passages through both 2A/1A CIs are less efficient due to their long distance from the major reaction path (**R3′**) and relatively high energies.

3.4.3. Overall Directionality in Stable-Trans→Unstable-Cis Photoisomerization. As mentioned in section 3.3.3, the helical torsion of the molecular backbone and repulsion of the asymmetric substituents significantly "turn" and "push" the *stable-cis→unstable-trans* photoisomerization path toward one of the 2A/1A CIs over the other; therefore, the overall 1B→2A→1A in **R3** photoisomerization shows reasonable directionality. This is also true in the *stable-trans→unstable-cis* (**R3′**) isomerization, except the "direction of pushing" is reversed. As shown in Figure 6c,d, the *stable-trans→unstable-cis* reaction paths are "pushed" along the yellow broad arrows toward the (+θ,+φ) direction, in contrast to the (−θ,−φ) direction in reaction **R3**. Consequently, **CI$_{2A/1A}$(−91°)** is expected to be the preferred crossing between 2A/1A surfaces, and the **V+** reaction path (purple arrows) is the major path in the 2A→1A radiationless transition for the *stable-trans→unstable-cis* reaction. For the same reasons presented in section 3.3.3, we conclude that the nonadiabatic 1B→2A→1A transition in *stable-trans→unstable-cis* photoisomerization of molecular rotary motor **3** is also unidirectional.

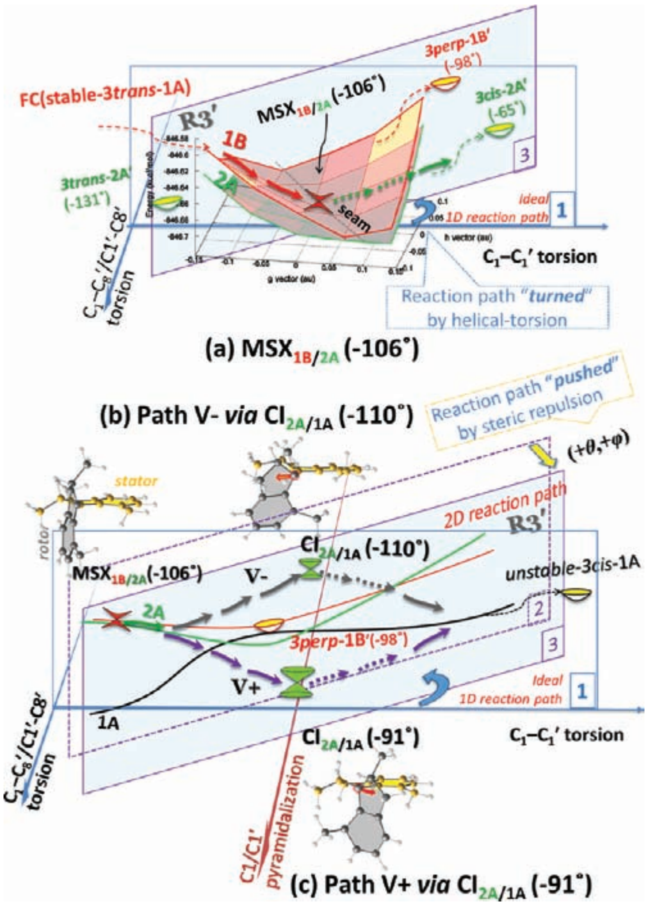

Figure 6. 1B/2A nonadiabatic reaction paths **R3′** via (a) **MSX$_{1B/2A}$(−106°)**, the 2A/1A pyramidalization path, (b) **V−** via **CI$_{2A/1A}$(−110°)**, and (c) **V+** via **CI$_{2A/1A}$(−91°)** originating from the **R3′** path. See caption of Figure 5 for details; a detailed illustration including the ***g*** and ***h*** vectors and all linear extrapolated 2D PESs is provided in Figure S6.

3.5. Overall Preferred Pathways for Photoisomerization of Molecular Motor 3.

Summarizing the findings of the preceding sections, we present the overall mechanism of the preferred photoisomerization pathways for the two key processes of molecular motor **3**: (*P,P*)-*stable-cis*→(*M,M*)-*unstable-trans*-**3**, step 1 of Figure 1, and (*P,P*)-*stable-trans*→(*M,M*)-*unstable-cis*-**3**, step 3 of Figure 1, as summarized in panels a and b in Figure 7, respectively. The photoisomerization processes follow the three-state multi-coordinate mechanism. The molecule excited in the 1B state first efficiently

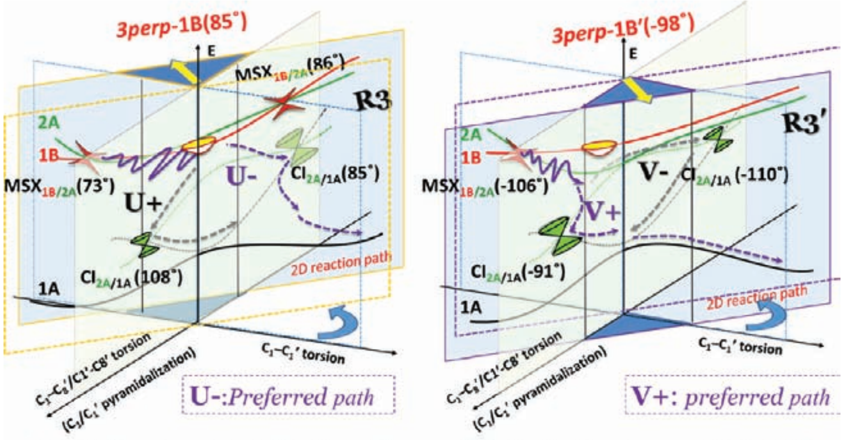

(a) *stable-cis* → *unstable-trans*-**3** **(b)** *stable-trans* → *unstable-cis*-**3**

Figure 7. Proposed mechanisms of (a) the *stable-cis*→*unstable-trans*-**3** (step 1 of Figure 1) and (b) the *stable-trans*→*unstable-cis*-**3** (step 3 of Figure 1) photoisomerizations, illustrated with the potential energy profiles in the vicinity of **3*perp*-1B** (θ = 85°) and **3*perp*-1B′** (θ = −98°) intermediate, respectively. The preferred paths are shown in purple and unfavorable paths in dark-gray dashed lines. For details, see Figure 5.

comes down to the 2A state through the 1B/2A seams along the C1−C1′ and C1−C8 (C1′−C8′) helical-torsional coordinates, then follows the C1/C1′ pyramidalization coordinate to preferentially cross one of the 2A/1A CIs and return to the ground-state PES.

It may be worth mentioning that although we maintained the C_2 symmetry and used the 2D reaction path and the C1/C1′ pyramidalization 2A/1A crossings as two intersecting planes to explain the reaction mechanism, this does not mean that the reaction necessarily follows one coordinate and then the other. In real trajectories, these coordinates are expected to participate in the photoisomerization reaction cooperatively and may give more complex dynamics than depicted in the present paper.

4. CONCLUSIONS

The photoisomerization of stiff stilbene molecular rotary motor **3**, a helical overcrowded alkene, has been calculated at the CASPT2//CASSCF level of theory. The unidirectionality of the C═C rotation in the photoisomerization processes, namely, (*P,P*)-*stable-cis*→(*M,M*)-*unstable-trans* and (*P,P*)-*stable-trans*→(*M,M*)-*unstable-cis*, can be rationalized by both the sloped nature of the excited-state 1B PESs and directional excited- to ground-state nonadiabatic transitions. The MEPs of these two processes (especially the 1B MEPs) are well-separated on the involved PESs and have remarkably steep slopes, which generates the directional motion and drives C═C bond rotation unidirectionally in the excited-state PES. The unidirectionality of the C═C rotation is also controlled by the locations and characters of the crossings, especially those of the 2A/1A CIs. The reactive molecules, along the cooperative C1−C1′ and C1−C8 (C1′−C8′) torsional coordinates, preferably approach one of the 2A/1A CIs, which, to a large extent, maintains the velocity of the trajectory and the direction of the rotation, consequently resulting in the unidirectional non-adiabatic reaction paths.

■ ASSOCIATED CONTENT

Ⓢ Supporting Information

Figures S1−S6, and Cartesian coordinates for the key structures of stilbenes **1**−**3**. This material is available free of charge via the Internet at http://pubs.acs.org.

■ AUTHOR INFORMATION

Corresponding Author

morokuma@fukui.kyoto-u.ac.jp

Notes

The authors declare no competing financial interest.

■ ACKNOWLEDGMENTS

We are grateful to Dr. Lung Wa Chung and Satoshi Maeda for helpful discussions. This work is in part supported by Japan Science and Technology Agency with a Core Research for Evolutional Science and Technology grant in the Area of High Performance Computing for Multiscale and Multiphysics Phenomena. The computational resource at Research Center of Computer Science at the Institute for Molecular Science is also acknowledged.

■ REFERENCES

(1) (a) Schliwa, M.; Woehlke, G. *Nature* **2003**, *422*, 759−765. (b) Kinbara, K.; Aida, T. *Chem. Rev.* **2005**, *105*, 1377−1400. (c) Rayment, I.; Holden, H. M.; Whittaker, M.; Yohn, C.; Lorenz, M.; Holmes, K. C.; Milligan, R. A. *Science* **1993**, *261*, 58−65. (d) Abrahams, J. P.; Leslie, A. G. W.; Lutter, R.; Walker, J. E. *Nature* **1994**, *370*, 621−628. (e) Noji, H.; Yasuda, R.; Yoshida, M.; Kinosita, K. Jr. *Nature* **1997**, *386*, 299−302.

(2) Leigh, D. A.; Wong, J. K. Y.; Dehez, F.; Zerbetto, F. *Nature* **2003**, *424*, 174−179.

(3) Kelly, T. R.; De Silva, H.; Silva, R. A. *Nature* **1999**, *401*, 150−152.

(4) (a) Feringa, B. L. *Acc. Chem. Res.* **2001**, *34*, 504−513. (b) Stoddart, J. F. *Acc. Chem. Res.* **2001**, *34*, 410−411. (c) Kay, E. R.; Leigh, D. A.; Zerbetto, F. *Angew. Chem., Int. Ed.* **2007**, *46*, 72−191. (d) Feringa, B. L. *J. Org. Chem.* **2007**, *72*, 6635−6652. (e) Balzani, V.; Credi, A.; Venturi, M. *Chem. Soc. Rev.* **2009**, *38*, 1542−1550. (f) Michl, J.; Sykes, E. C. H. *ACS Nano* **2009**, *3*, 1042−1048.

(5) (a) Koumura, N.; Zijlstra, R. W. J.; van Delden, R. A.; Harada, N.; Feringa, B. L. *Nature* **1999**, *401*, 152−155. (b) Koumura, N.; Geertsema, E. M.; van Gelder, M. B.; Meetsma, A.; Feringa, B. L. *J. Am. Chem. Soc.* **2002**, *124*, 5037−5051. (c) Pijper, D.; van Delden, R. A.; Meetsma, A.; Feringa, B. L. *J. Am. Chem. Soc.* **2005**, *127*, 17612−17613. (d) Pollard, M. M.; ter Wiel, M. K. J.; van Delden, R.; Vicario, J.; Koumura, N.; van den Brom, C.; Meetsma, A.; Feringa, B. *Chem.—Eur. J.* **2008**, *14*, 11610. (e) van Delden, R. A.; ter Wiel, M. K. J.; Pollard, M. M.; Vicario, J.; Koumura, N.; Feringa, B. L. *Nature* **2005**, *437*, 1337−1340. (f) Klok, M.; Boyle, N.; Pryce, M. T.; Meetsma, A.; Browne, W. R.; Feringa, B. L. *J. Am. Chem. Soc.* **2008**, *130*, 10484−

10485. (g) London, G.; Carroll, G. T.; Fernandez Landaluce, T.; Pollard, M. M.; Rudolf, P.; Feringa, B. L. *Chem. Commun.* **2009**, 1712−171. (h) Ruangsupapichat, N.; Pollard, M. M.; Harutyunyan, S. R.; Feringa, B. L. *Nat. Chem.* **2010**, *3*, 53−60. (i) Wang, J.; Feringa, B. L. *Science* **2011**, *331*, 1429−1432.

(6) (a) Michl, J.; Bonacić-Koutecký, V. *Electronic Aspects of Organic Photochemistry*; Wiley: New York, 1990. (b) Bernardi, F.; Olivucci, M.; Robb, M. A. *Chem. Soc. Rev.* **1996**, *25*, 321. (c) Köppel, H.; Domcke, W. In *Encyclopedia of Computational Chemistry*; Schleyer, P. v. R., Ed.; Wiley: New York, 1998. (d) Fuss, W.; Lochbrunner, S.; Müller, A. M.; Schikarski, T.; Schmid, W. E.; Trushin, S. A. *Chem. Phys.* **1998**, *232*, 161−174.

(7) Torras, J.; Rodríguez-Ropero, F.; Bertran, O.; Alemán, C. *J. Phys. Chem. C* **2009**, *113*, 3574−3580.

(8) (a) Kazaryan, A; Filatov, M. *J. Phys. Chem. A* **2009**, *113*, 11630−11634. (b) Kazaryan, A.; Kistemaker, J. C. M.; Schäfer, L. V.; Browne, W. R.; Feringa, B. L.; Filatov, M. *J. Phys. Chem. A* **2010**, *114*, 5058−5067. (c) Kazaryan, A.; Lan, Z.; Schäfer, L. V.; Thiel, W.; Filatov, M. *J. Chem. Theory Comput.* **2011**, *7*, 2189−2199.

(9) Pollard, M. M.; Meetsma, A.; Feringa, B. L. *Org. Biomol. Chem.* **2008**, *6*, 507−512.

(10) Pérez-Hernández, G.; González, L. *Phys. Chem. Chem. Phys.* **2010**, *12*, 12279−12289.

(11) Roos, B. O. In *Ab Initio Methods in Quantum Chemistry II*; Lawley, K. P., Ed.; Advances in Chemical Physics 69; John Wiley & Sons: New York, 1987; pp 399− 446.

(12) Finley, J.; Malmqvist, P.-Å.; Roos, B. O.; Serrano-Andres, L. *Chem. Phys. Lett.* **1998**, *288*, 299.

(13) Ditchfield, R.; Hehre, W. J.; Pople, J. A. *J. Chem. Phys.* **1971**, *54*, 724−728.

(14) (a) Waldeck, D. H. *Chem. Rev.* **1991**, *91*, 415−436. (b) Papper, V. *J. Photochem. Photobiol. A: Chemistry* **2001**, *140*, 39−52.

(15) Poli, R.; Harvey, J. N. *Chem. Soc. Rev.* **2003**, *32*, 1.

(16) Yarkony, D. R. *Rev. Mod. Phys.* **1996**, *68*, 985−1013.

(17) Celani, P.; Werner, H.-J. *J. Chem. Phys.* **2000**, *112*, 5546.

(18) Werner, H.-J.; Knowles, P. J.; Lindh, R. http://www.molpro.net; MOLPRO 2006.1, a package of ab initio programs designed by Werner, H.-J.; Knowles, P. J., Universität Stuttgart, Germany, and Cardiff University, Cardiff, U.K., 2006.

(19) Roos, B. O.; Andersson, K. *Chem. Phys. Lett.* **1995**, *245*, 215−223.

(20) (a) Syage, J. A.; Lambert, W. R.; Felker, P. M.; Zewail, A. H. *Chem. Phys. Lett.* **1982**, *88*, 266. (b) Fuss, W.; Kosmidis, C.; Schmid, W. E.; Trushin, S. A. *Angew. Chem., Int. Ed.* **2004**, *43*, 4178−4182. (c) Takeuchi, S.; Ruhman, S.; Tsuneda, T.; Chiba, M.; Taketsugu, T.; Tahara, T. *Science* **2008**, *322*, 1073.

(21) (a) Bearpark, M. J.; Bernardi, F.; Cliford, S.; Olivucci, M.; Robb, M. A.; Vreven, T. *J. Phys. Chem. A* **1997**, *101*, 3841−3847. (b) Molina, V.; Merchan, M.; Roos, B. O. *J. Phys. Chem. A* **1997**, *101*, 3478. (c) Gagliardi, L.; Orlandi, G.; Molina, V.; Malmqvist, P. A.; Roos, B. O. *J. Phys. Chem. A* **2002**, *106*, 7355. (d) Quenneville, J.; Martinez, T. J. *J. Phys. Chem. A* **2003**, *107*, 829−837. (e) Improta, R.; Santoro, F. *J. Phys. Chem. A* **2005**, *109*, 10058.